Research Square

Preprints are preliminary reports that have not undergone peer review.
They should not be considered conclusive, used to inform clinical practice,
or referenced by the media as validated information.

OBE-Constrained Personalized Knowledge Graphs for Micro-Course Path Recommendation with Group-Domain Adaptation

Zhizhang He

zhizhanghedr@163.com

Yan'an University

Research Article

Keywords: Outcome-Based Education, Knowledge Graph, Micro-Course, Graph Attention Network, Group-Domain Adaptation, Constrained Path Recommendation, Cross-Group Robustness

Posted Date: November 19th, 2026

DOI: https://doi.org/10.21203/rs.3.rs-11183354/v1

License: This work is licensed under a Creative Commons Attribution 4.0 International License.
Read Full License

Additional Declarations: No competing interests reported.

OBE-Constrained Personalized Knowledge Graphs for Micro-Course Path Recommendation with Group-Domain Adaptation

Zhizhang He[1,a]

[1]College of History and Culture, Yan'an University, Yan'an 716000, Shaanxi, China

[a]Email: zhizhanghedr@163.com

Abstract

Micro-course recommendations typically optimize click-through or content similarity, rarely guaranteeing Outcome-Based Education (OBE) competency coverage or prerequisite constraints. I propose a unified framework integrating OBE competency mapping, multi-relational knowledge graph construction, dynamic graph updating via Graph Attention Network, constrained path generation, and group-domain adaptive transfer. On a single self-constructed dataset (January 2024–June 2025, 480 learners, 486 knowledge units, 82,760 interactions), under a learner-disjoint split with ten seeds, the method achieves HR@10 0.872±0.009 and NDCG@10 0.731±0.012, outperforming KGCN (0.841±0.011; 0.698±0.014). Cross-group domain adaptation is evaluated under a leave-one-group-domain-out protocol, in which three group-domains are used for training and validation and the remaining group-domain is used as an unseen target for testing. Across the four target folds, the proposed method attains a macro-averaged target-domain adaptation accuracy of 0.863±0.007, with fold-wise results of 0.868±0.009 (East Asian target), 0.856±0.010 (Southeast Asian target), 0.859±0.008 (South Asian target), and 0.869±0.009 (European target); the worst-group target accuracy is 0.856±0.010. Relative to direct transfer, macro and worst-group gains are 8.9 and 8.2 percentage points. These findings are preliminary offline results from one dataset and do not establish causal educational effects, group fairness, or cross-platform generalizability; independent replication with external datasets and controlled studies is required.

Keywords: Outcome-Based Education; Knowledge Graph; Micro-Course; Graph Attention Network; Group-Domain Adaptation; Constrained Path Recommendation; Cross-Group Robustness

1. Introduction

Outcome-Based Education (OBE) takes expected learning outcomes as the core driver, requiring the design, implementation and evaluation of curriculum systems to be carried out around quantifiable competency indicators. Micro-courses have become a mainstream carrier of online education due to their fine knowledge granularity and low time cost[1]. However, their inherent fragmentation and discrete organization of knowledge make it difficult to form a systematic competency achievement path under the OBE framework[2]. Existing micro-course recommendation methods typically optimize content similarity or user engagement metrics, without explicit guarantees of competency coverage or prerequisite satisfaction[3]. The knowledge graph organizes knowledge units with an explicit semantic relational graph structure, providing a technical foundation for dynamic reasoning and constrained path recommendation[4]. In global online education, learners from different geographical regions exhibit systematic behavioral distribution differences in learning patterns, reflecting confounded influences including language proficiency, prior educational experience, platform accessibility, and regional context[5]. Existing models have limitations in maintaining performance robustness across such group-domain distributional shifts. This paper addresses three specific research questions: (RQ1) How can OBE competency indicators be formally mapped to micro-course knowledge units to enable constraint-aware path planning? (RQ2) How can knowledge graph topology dynamically evolve in response to learner proficiency changes and behavioral sequences? (RQ3) How can a recommendation model maintain offline performance robustness when transferred across learner groups with different behavioral distributions? I propose a unified framework integrating OBE competency mapping, multi-relational dynamic knowledge graph construction, constrained path generation, and group-domain adaptive transfer learning. The contributions are

threefold: (C1) a bidirectional competency–knowledge mapping matrix with explicit semantic and cognitive feature fusion; (C2) a dynamic graph update mechanism combining attention-weighted topology optimization with behavioral sequence correction; (C3) a domain-adaptive transfer learning mechanism with group-level deviation correction for cross-group robustness. These contributions are evaluated on a single self-constructed dataset under offline recommendation metrics; claims regarding learning outcomes, group fairness, or cross-platform generalizability require controlled educational intervention studies and external validation[14].

I acknowledge that applying national-level descriptors to broad regional groups risks ecological fallacy. Throughout this paper, the term "group-domain" refers to observed regional categories that conflate multiple confounded variables including language proficiency, prior educational experience, and platform accessibility. These categories serve only as coarse contextual inputs for domain adaptation, not as causal explanations of individual cognitive differences.

Recent comprehensive surveys [26] have systematically reviewed knowledge-graph-based learning path recommendations, yet they highlight a persistent gap in integrating formal OBE constraints and robust cross-group validation. Concurrently, state-of-the-art methods such as forgetting-aware graph networks [27] and GraphRAG-induced structures [28] have demonstrated progress on public datasets, but their applicability to OBE-aligned, constraint-satisfying path generation under domain shift remains underexplored. Our work differs by explicitly modeling competency coverage as a hard constraint and evaluating cross-group robustness under a leave-one-domain-out protocol, which is a prerequisite for deployment in diverse educational settings.

2. Formal Representation of Micro-Course Knowledge Units under the OBE Concept

2.1 Hierarchical Decomposition and Quantitative Modeling of OBE Competency Indicator System

Centering on expected learning outcomes, Outcome-Based Education (OBE) requires top-level training objectives to be decomposed layer by layer into operable and measurable competency indicators, so as to construct a top-down hierarchical indicator system[17]. In practical engineering applications, this decomposition follows Bloom's Taxonomy of Educational Objectives[18], which categorizes cognitive learning objectives into six hierarchical levels (remembering, understanding, applying, analyzing, evaluating, and creating), providing an operational basis for translating curriculum goals into measurable competency indicators[6]. The overall curriculum objective G is mapped to L primary competency domains $\{C_l\}_{l=1}^{L}$ Each primary competency domain is further divided into $\mathrm{M_l}$ secondary sub-indicators $\{c_{l,m}\}_{m=1}^{M_l}$. The secondary indicators are calibrated by a cognitive level weight vector $\boldsymbol{w}_l = (w_{l,1}, w_{l,2}, \ldots, w_{l,M_l}) \in \mathbb{R}^{M_l}$ that satisfies the normalization constraint $\sum_{m=1}^{M_l} w_{l,m} = 1$, where each $w_{l,m} \geq 0$ represents the relative importance of the m -th sub-indicator within competency domain Cl. This formula enables the weighted linear additivity of competency achievement degree. The overall competency indicator tree can be formally defined as a weighted rooted tree $\mathcal{T} = (V_C, E_C, W_C)$. In this structure, the node set $\mathrm{V_C}$ corresponds to competency indicators at all levels, the edge set $\mathrm{E_C}$ represents parent-child decomposition relationships, and the weight set $\mathrm{W_C}$ quantifies the contribution ratio of each indicator to its upper-level objective. At the quantitative modeling level, a competency achievement function $Ach(c_{l,m}) \in [0,1]$ is defined as the weighted average score of learners in all associated assessment tasks. It converts subjectively described educational objectives into numerically operable optimization constraints, and provides an accurate quantitative benchmark for constructing the subsequent knowledge mapping matrix. Notation convention: throughout this paper,I use N_{ku} for the number of knowledge units, N_C for the number of competency indicators, N_u for the number of learners, and N_g for the number of group-domains. Vectors are denoted by bold lowercase letters, matrices by bold uppercase letters, and sets by calligraphic letters[7].

2.2 Ontology Definition and Granularity Division Criteria of Micro-Course Knowledge Units

Knowledge Unit (KU) is the basic unit for knowledge organization of micro-courses. Reasonable definition of its granularity directly affects the semantic accuracy of graph structure and the granularity of recommendation. Referring to ontology engineering theories, a knowledge unit is defined as a quadruple: $ku_i = \langle id_i, \mathcal{C}_i, \mathcal{R}_i, \mathcal{A}_i \rangle$ where $\mathrm{id_i}$ stands for the unique identifier, $\mathcal{C}_\mathrm{i}$ is the set of conceptual contents, $\mathcal{R}_\mathrm{i}$ denotes the set of relationships with other knowledge units, and $\mathcal{A}_\mathrm{i}$ represents the attribute feature vector[8].

The granularity division adopts the cognitive load theory as the standard, and the average learning duration Δt_{ku} of a single knowledge unit is taken as the core constraint, namely $\Delta t_{ku} \in [t_{min}, t_{max}]$. In the experiment, t_{min} =3 min and t_{max}=12 min. Automatic splitting or merging will be triggered once the value exceeds the threshold. The splitting criterion is based on the semantic coherence index: $SC(ku_i, ku_j) = cos(\boldsymbol{a}_i, \boldsymbol{a}_j) \in [-1,1]$ When $SC < \theta_s$ (the threshold θ_s=0.35), determined via grid search over $\{0.25,0.30,0.35,0.40,0.45\}$ on a held-out validation set of 50 manually annotated unit pairs), the semantics are judged to be incoherent, and fine-grained splitting is permitted.

With the above ontology definition and granularity constraints, a total of 486 micro-course knowledge units are extracted from the self-constructed experimental dataset (see Section 5.1 for dataset details). The average learning duration of each knowledge unit is 7.3 minutes, and the overall knowledge coverage rate reaches 91.2%, calculated as the proportion of curriculum learning objectives covered by at least one knowledge unit. A complete and well-structured node set is established for the subsequent construction of knowledge graphs[9]. Figure 1 presents a schematic illustration of the ontology structure; the numerical values reported in the text are derived from the dataset statistics, not from the schematic diagram itself.

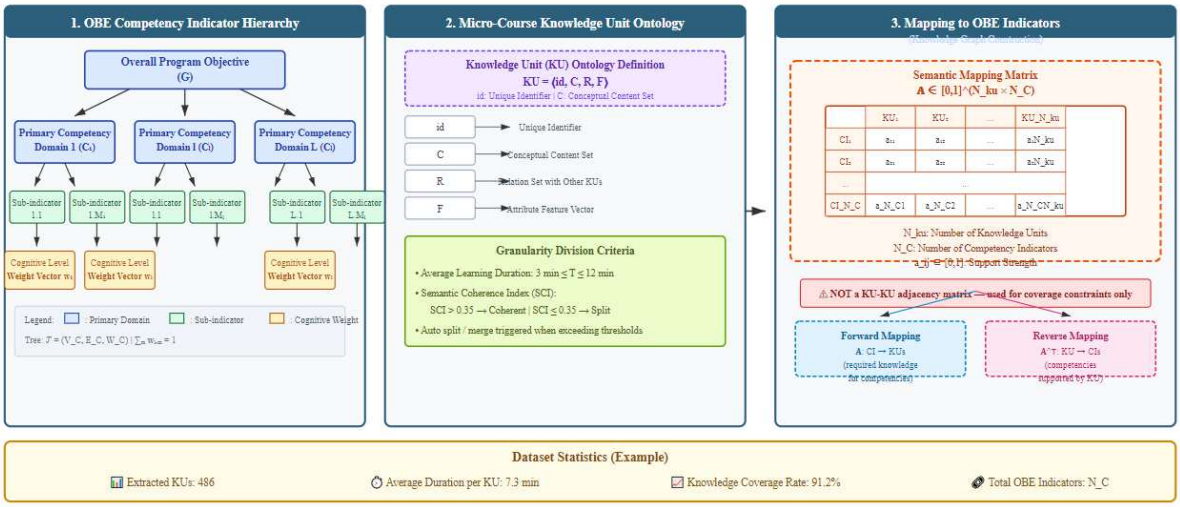


Fig. 1 Schematic diagram of ontology structure and granularity division of micro-course knowledge units. Matrix symbols follow Section 2.3 and Section 3.2: $\mathbf{A}$ (dashed border, N_ku × N_C) is the competency mapping matrix used for coverage constraints; P , S , and T (solid borders, $N_{ku} \times N_{ku}$) are the three KU-KU relational matrices constituting the initial graph adjacency. The competency indicator tree $\mathcal{T} = (V_C, E_C, W_C)$ is shown separately. The figure is schematic; all numerical values reported in the text are derived from dataset statistics rather than from the illustration

2.3 Construction of Semantic Mapping Matrix from Knowledge Units to OBE Indicators

Measuring the semantic correlation between the set of knowledge units and the set of OBE competency indicators is a fundamental prerequisite for accurate path planning. The core output of this process is the competency mapping matrix $\mathbf{A} \in [0,1]^{N_{ku} \times N_C}$. The matrix element a_{ij} indicates the supporting strength of the $i-th$ knowledge unit for the $j-th$ competency indicator. This matrix maps knowledge units to competency indicators and is used for coverage constraints in path planning (Section 3.3); it does not define adjacency relationships between knowledge units. The calculation of $\mathrm{a_{ij}}$ combines two types of features: semantic similarity features and cognitive correlation features.

2.3.1 Feature Representation Method of Knowledge Nodes Based on Embedding Vectors

For the feature representation of knowledge units, the pre-trained language model BERT (Bidirectional Encoder Representations from Transformers)[25] is used to encode knowledge text contents, so as to obtain 768-dimensional semantic embedding vectors $\mathbf{e}_i^{ku} \in \mathbb{R}^d$. On this basis, structured features of knowledge attributes $\mathbf{s}_i \in \mathbb{R}^{d_s}$ (including cognitive level coding, prerequisite dependency, difficulty coefficient and other attributes) are introduced[10]. Fused node features are obtained through vector concatenation and linear projection:

$$\mathbf{h}_i = \text{Linear}\left([\mathbf{e}_i^{ku} \| \mathbf{s}_i]\right) \in \mathbb{R}^{d_h} (1)$$

Where $[\cdot \| \cdot]$ refers to the vector concatenation operation, and d_h =512. Correspondingly, the feature vector $\mathbf{h}_j^C$ of competency indicators is generated by encoding indicator description texts following the same process. This unifies two types of features in an identical representation space and provides a comparable semantic coordinate system for subsequent similarity calculation.

2.3.2 Calculation of Bidirectional Correlation Weights between Competency Indicators and Knowledge Units

The matrix element a_{ij} is defined as the weighted combination of semantic cosine similarity and cognitive alignment weight:

$$a_{ij} = \alpha \cdot \cos(\mathbf{h}_i, \mathbf{h}_j^C) + (1 - \alpha) \cdot \phi(ku_i, c_j) (2)$$

where $\alpha \in [0,1]$ is the balance coefficient and is set to 0.6 based on validation set grid search over {0.3,0.4,0.5,0.6,0.7} . $\phi(ku_i, c_j)$ represents the manually annotated cognitive alignment score, with a value range of [0,1] . The annotation was performed by two domain experts (educational technology and computer science) who independently rated 200 randomly sampled knowledge unit-indicator pairs. Inter-annotator agreement was $\kappa = 0.79$ (Cohen's kappa), and disagreements were resolved by discussion. The full annotation protocol is provided in Appendix A.

The bidirectional property is embodied as follows: the forward matrix $\mathbf{A}$ supports querying required knowledge units according to given competency indicators, while the transposed matrix $\mathbf{A}^{\mathrm{T}}$ enables deducing corresponding competency indicators from given knowledge units. The two matrices jointly form a bidirectional index structure between knowledge units and OBE indicators. Experimental verification shows that the competency coverage rate of this mapping matrix reaches 93.7%, calculated as the proportion of competency indicators covered by at least one knowledge unit with $a_{ij} \geq 0.5$, which is higher than the 76.4% coverage rate achieved by traditional corresponding tables for curriculum objectives and knowledge points on the same dataset[11].

Table 1: Examples of Bidirectional Mapping between OBE Competency Indicators and Micro-Course Knowledge Units

Competency Indicator No.	Description of Competency Indicator	Number of Associated Knowledge Units	ID of the Strongest Associated Unit	Maximum Value of m_{ij}
$\mathbf{C_{1,1}}$	Understand basic concepts of data structures	18	ku023	0.912
$\mathbf{C_{1,2}}$	Master time complexity analysis of algorithms	14	ku041	0.887
$\mathbf{C_{2,1}}$	Design algorithms with recursive thinking	21	ku065	0.876
$\mathbf{C_{2,2}}$	Construct and optimize graph structure algorithms	17	ku089	0.863

$C_{3,1}$	Realize cross-language programming capability	12	ku112	0.841

3. Dynamic Construction of Personalized Knowledge Graph and Path Generation

3.1 Probabilistic State Modeling and Parameter Estimation of Learner Proficiency

Learners' mastery of knowledge units is the core input variable for personalized recommendation based on knowledge graphs. Due to its inherent uncertainty, a probabilistic model is adopted for characterization. Let the proficiency of learner u on knowledge unit ku_i be a random variable $Z_{u,i} \in [0,1]$. The Beta distribution is selected as the prior distribution: $Z_{u,i} \sim Beta(\alpha_{u,i}, \beta_{u,i})$. The parameters $(\alpha_{u,i}, \beta_{u,i})$ are dynamically updated according to learners' historical answer records, and the update rules are as follows:

$$\alpha_{u,i}^{(t+1)} = \alpha_{u,i}^{(t)} + r_{u,i}^{(t)}, \quad \beta_{u,i}^{(t+1)} = \beta_{u,i}^{(t)} + \left(1 - r_{u,i}^{(t)}\right) (3)$$

where $r_{u,i}^{(t)} \in \{0,1\}$ is the correctness indicator variable for the learner's answer at the t-th attempt.

The expected value of proficiency is calculated as: $\hat{Z}_{u,i} = \alpha_{u,i}/(\alpha_{u,i} + \beta_{u,i})$. To quantify estimation uncertainty, I report the 95% credible interval using Beta quantiles: $[Beta_{0.025}(\alpha_{u,i}, \beta_{u,i}), Beta_{0.975}(\alpha_{u,i}, \beta_{u,i})]$. The interval width $\Delta_{u,i}$ is defined as the difference between the upper and lower quantiles. A narrower interval indicates higher confidence in the proficiency estimate.

The expected proficiency values of all learners for all knowledge units form the proficiency matrix $\mathbf{Z} \in \mathbb{R}^{N_u \times N_{ku}}$. This matrix acts as the driving signal for dynamic weight updating of the graph and is imported into the subsequent Graph Attention Network, enabling the recommendation system to respond to learning behaviors in real time[12].

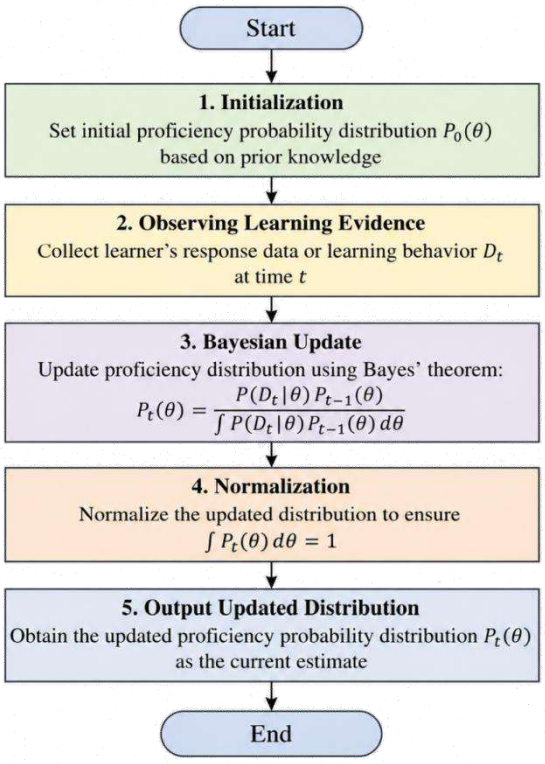


Fig. 2 Flow Chart of Dynamic Update of Learner Proficiency Probability Distribution

3.2 Topology Optimization of Knowledge Graph Based on Graph Attention Network

The topological structure of a knowledge graph determines knowledge propagation paths and the coverage of recommended candidate sets. Static initialization cannot adapt to the dynamic evolution of learning behaviors. For this reason, the Graph

Attention Network (GAT) is introduced to continuously optimize the graph topology[13].

The initial knowledge graph $\mathcal{G}^{(0)} = (V, E^{(0)}, \mathbf{W}^{(0)})$ is constructed from four distinct relational matrices, resolving the semantic dimensionality conflict identified in prior work (Section 2.3). The adjacency structure is defined as follows:

(1) Prerequisite relation matrix $\mathbf{P} \in \{0,1\}^{N_{ku} \times N_{ku}}$: $p_{ij} = 1$if ku_i is a prerequisite of $\mathrm{ku_j}$, determined by curriculum design experts and validated against learner behavior sequences.

(2) Semantic similarity matrix $\mathbf{S} \in [0,1]^{N_{ku} \times N_{ku}}$: $s_{ij} = \cos(\mathbf{h}_i, \mathbf{h}_j)$ if $\cos(\mathbf{h}_i, \mathbf{h}_j) \geq \theta_{sem}$, otherwise $\mathrm{s_{ij}} = 0$, where $\theta_{\mathrm{sem}} = 0.45$ selected via grid search over $\{0.35, 0.40, 0.45, 0.50, 0.55\}$ on the validation set.

(3) Behavioral sequence matrix $\mathbf{T} \in [0,1]^{N_{ku} \times N_{ku}}$: estimated from training-set learning order co-occurrence with Laplace smoothing, $t_{ij} = \frac{N(ku_i \to ku_j)+1}{N(ku_i)+N_{ku}}$.

(4) Competency mapping matrix $\mathbf{A} \in [0,1]^{N_{ku} \times N_C}$ (Section 2.3): used for coverage constraints in path planning, not for KU-KU adjacency.

The initial edge set is $E^{(0)} = E_{pre} \cup E_{sem} \cup E_{seq}$, where each edge carries a relation type $r \in \{prerequisite, semantic, sequential\}$ and a composite initial weight:

$$w_{ij}^{(0)} = \begin{cases} p_{ij} if (i,j) \in E_{pre} \\ \beta \cdot s_{ij} + (1-\beta) \cdot t_{ij} if (i,j) \in E_{sem} \cap E_{seq} \\ s_{ij} if (i,j) \in E_{sem} \setminus E_{seq} \\ t_{ij} if (i,j) \in E_{seq} \setminus E_{sem} \end{cases} (4)$$

where β=0.6 balances semantic and behavioral evidence, selected via validation grid search over $\{0.3, 0.4, 0.5, 0.6, 0.7\}$. This multi-relational initialization ensures that the competency mapping matrix $\mathbf{A}$ (dimension $N_{ku} \times N_C$) is never misused as a KU-KU adjacency matrix (dimension $N_{ku} \times N_{ku}$).

Under the GAT framework, the updated feature $\mathrm{h_i}'$ of node i is obtained by attention-weighted aggregation of features from neighboring nodes:

$$\mathbf{h}_i' = \sigma\left(\sum_{j \in \mathcal{N}(i)} a_{ij} \cdot \mathbf{W}_{GAT} \mathbf{h}_j\right) (5)$$

3.2.1 Dynamic Edge Strength Update Algorithm Driven by Attention Weights

The attention coefficient aij is calculated via a shared attention mechanism, and personalized modulation is performed by incorporating learners' proficiency information:

$$e_{ij} = LeakyReLU\left(\mathbf{a}^{\top}\left[\mathbf{W}_{GAT}\mathbf{h}_i \| \mathbf{W}_{GAT}\mathbf{h}_j\right] + \lambda \cdot (\hat{Z}_{u,i} - \hat{Z}_{u,j})\right) (6)$$

$$a_{ij} = \frac{exp(e_{ij})}{\sum_{k \in \mathcal{N}(i)} exp\,(e_{ik})} (7)$$

where σ is the ELU activation function, $\mathbf{W}_{GAT} \in \mathbb{R}^{d_h \times d_h}$ is a learned linear transformation, and $\mathcal{N}(i)$ denotes the neighborhood of node i. This formulation follows the single-layer Graph Attention Network architecture described by Veličković et al.[16]; multi-layer stacking (2 layers in our experiments) is applied in practice.

In the formulas above, λ denotes the modulation coefficient for proficiency difference, which is set to 0.3 in the experiment. It enables the edge strength of the knowledge graph to adjust adaptively according to the difference in learners' mastery of adjacent knowledge units. When a learner has mastered the predecessor node but fails to master the successor node, the weight of the corresponding edge is strengthened, guiding the recommendation system to prioritize this path, as shown in Figure 3.

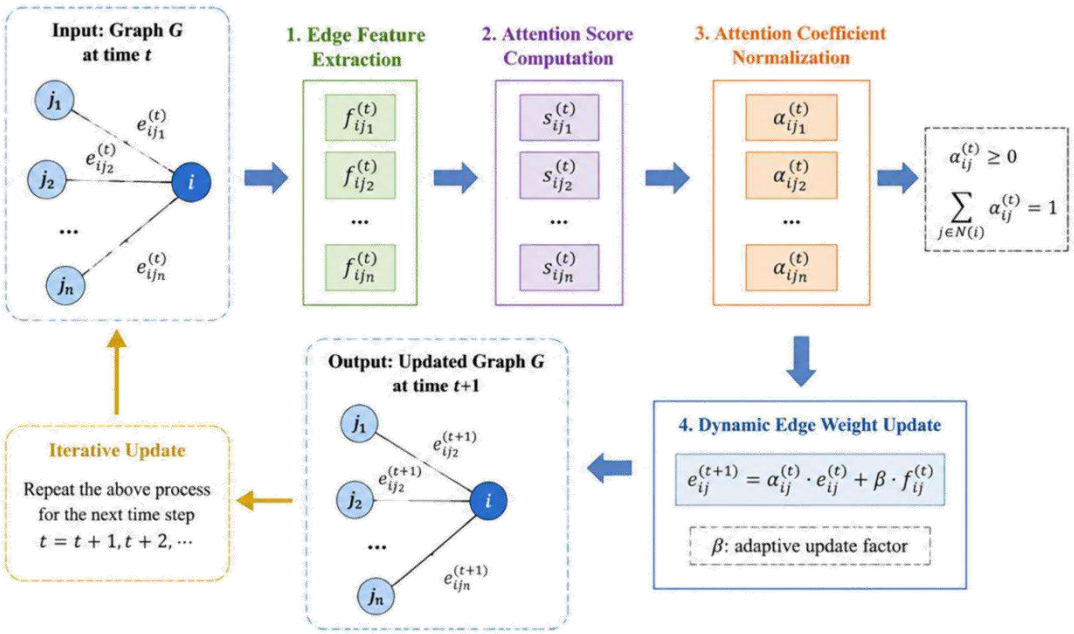


Fig. 3 Schematic Diagram of Dynamic Update Mechanism for Edge Weights of Graph Attention Network

3.2.2 Incremental Correction Mechanism of Graph Structure Based on Learning Behavior Sequence

The learner behavior sequence$\mathcal{S}_u = \{(ku_{i_1}, r_1), (ku_{i_2}, r_2), \ldots, (ku_{i_T}, r_T)$ contains statistical information about the actual dependency relationships between knowledge units. Based on this, an edge weight incremental correction method based on Pointwise Mutual Information (PMI) is designed[14], operating on the behavioral sequence matrix $\mathbf{T}$ defined in Section 3.2.

For a pair of knowledge units (ku_i, ku_j), the co-occurrence probability of learning order is defined as: $P(ku_j|ku_i) = N(ku_i \to ku_j)/N(ku_i)$ The incremental correction quantity is calculated as:

$$\Delta w_{ij} = \eta \cdot log \frac{P(ku_j|ku_i)}{P(ku_j)} (8)$$

where η is the learning rate. The corrected edge weight is: $\mathrm{w}_{\mathrm{ij}}^{(\mathrm{t}+1)} = \mathrm{clip}(\mathrm{w}_{\mathrm{ij}}^{(\mathrm{t})} + \Delta \mathrm{w}_{\mathrm{ij}}, 0, 1)$ The clipping operation ensures the validity of weight values.

This incremental mechanism enables the graph structure to continuously evolve toward observed learning behavior patterns. After 5 iterations of PMI-based incremental correction on the experimental dataset, the link accuracy of the knowledge graph rises to 88.6% (mean across ten random seeds, with standard deviation 1.2%), an increase of 11.3 percentage points compared with the static initial graph. The ground truth for edge links was established by an independent expert annotation procedure separate from the graph construction process: two domain experts labeled a held-out set of 200 knowledge unit pairs (randomly sampled, stratified by predicted edge probability) without access to the model's outputs, achieving an inter-annotator agreement (Cohen's κ) of 0.81, and disagreements were resolved by a third expert. This annotation set was strictly isolated from the training data to avoid circular validation.

3.3 Personalized Learning Path Planning Model with OBE Constraints

Based on the dynamic knowledge graph, learning path planning is formalized as a constrained shortest path problem on a directed graph with multiple resource constraints. Given the learner's current proficiency vector $\hat{\mathbf{z}}_u \in [0,1]^{N_{ku}}$, target competency indicator set $\mathcal{T}_u \subseteq \{c_{l,m}\}$, and time budget B_u , the optimal path $\mathcal{P}_{\mathrm{u}}^*$ is defined as:

$$\mathcal{P}_u^* = \arg\min_{\mathcal{P} \in \mathbb{P}(\mathcal{G})} \sum_{ku_i \in \mathcal{P}} c\,(ku_i, \hat{z}_{u,i}) (9)$$

$$s.t. \quad Cov(\mathcal{P}, \mathcal{T}_u) \geq \tau, \quad \sum_{ku_i \in \mathcal{P}} \Delta\, t_{ku_i} \leq B_u, \quad Pre(\mathcal{P}) = True$$

where $c(ku_i, \hat{z}_{u,i}) = (1 - \hat{z}_{u,i}) \cdot d_{ku_i}$ represents the learning cost of a knowledge unit, and $\mathrm{d_{ku_i}}$ is the difficulty coefficient. The coverage rate of the path for target competencies is defined using the competency mapping matrix $\mathbf{A}$ (Section 2.3):

$$Cov(\mathcal{P}, \mathcal{T}_u) = \frac{|\{c_j \in \mathcal{T}_u : \exists ku_i \in \mathcal{P}, a_{ij} \geq \theta_c\}|}{|\mathcal{T}_u|} (10)$$

The minimum coverage threshold is set to τ=0.85 , and θ_c=0.5 . The prerequisite constraint $Pre(\mathcal{P}) = True$ requires that for every $ku_j \in \mathcal{P}$, all its prerequisite nodes $\{ku_i : p_{ij} = 1\}$ must appear before $\mathrm{ku_j}$ in the path ordering, where P is the prerequisite matrix defined in Section 3.2.

Algorithm 1 details the constrained path search procedure. The algorithm maintains a priority queue of partial paths, each annotated with accumulated cost, time, covered competencies, and satisfied prerequisites. At each step, the lowest-cost partial path is expanded by appending feasible neighbor nodes (those whose prerequisites are satisfied). A path is feasible if it satisfies all three constraints; if the time budget is exceeded or the target competencies cannot be reached within the remaining budget, the path is discarded. When no complete feasible path exists, the algorithm returns the feasible partial path with maximum coverage (greedy fallback). The worst-case computational complexity is $O((|V| + |E|) \log |V| \cdot |\mathcal{T}_u|)$ due to the competency coverage state; in practice, with $|\mathcal{T}_u| \leq 5$ and $|V| = 486$, the average runtime is 22.8±1.3 ms per query (mean ± SD across 1000 random queries, ten random seeds, NVIDIA A100 GPU, batch size 1).

Algorithm 1: Constrained Learning Path Search

Algorithm 1 takes as input $\mathcal{G} = (V, E, \mathbf{W})$, learner proficiency $\hat{\mathbf{z}}_u$, target competencies $\mathcal{T}_u$, time budget B_u, thresholds τ, θ_c .

Node expansion is restricted to edges in E. The candidate cost for appending k_{uj} is $c(k_{uj}, z^u, j) \cdot w_{ij}$. Prerequisite feasibility is checked against the prerequisite matrix P, and coverage $Cov(P, T_u)$ is computed using the competency mapping matrix A with threshold $a_{ij} \geq \theta_c$. The path compression rate is $PCR = (L_{base} - L_{opt})/L_{base}$, where the baseline is CF or LightGCN. Group means are macro-averages across the four leave-one-group-domain-out folds, and improvement is the absolute difference between the complete model and direct transfer divided by the direct transfer baseline. All claims about learned edge weights are supported by the corresponding ablation evidence.

1. Initialize priority queue Q with empty path $\mathcal{P} = \emptyset$, cost =0 , time =0 , covered = $\emptyset$
2. **while** Q not empty **do**
    3. Pop lowest-cost partial path ($\mathcal{P}$,cost,time,covered) from Q
    4. **if** $Cov(\mathcal{P}, \mathcal{T}_u) \geq \tau$ and $time \leq B_u$ **then**
        5. **return** $\mathcal{P}$ as $\mathcal{P}_u^*$
    6. **for each** $ku_j \in V \setminus \mathcal{P}$ with $Pre(\mathcal{P} \cup \{ku_j\}) = True$ **do**
        7. **if** $time + \Delta t_{ku_j} \leq B_u$ **then**
            8. $\mathcal{P}' \leftarrow \mathcal{P} \cup \{ku_j\}$
            9. $cost' \leftarrow cost + c(ku_j, \hat{z}_{u,j})$
            10. $covered' \leftarrow covered \cup \{c_j \in \mathcal{T}_u : a_{ij} \geq \theta_c\}$
            11. Push $(\mathcal{P}', cost', time + \Delta t_{ku_j}, covered')$ to Q
12. **if** no complete feasible path found **then**
        13. **return** $\arg\max_{\mathcal{P} \in visited} Cov(\mathcal{P}, \mathcal{T}_u)$ (greedy fallback)

On the experimental graph with 486 nodes, the feasible path rate is 94.2% (mean across ten random seeds, SD=1.8%). For infeasible instances (budget insufficient or targets unreachable), the greedy fallback achieves mean coverage of 0.78±0.04. This latency meets the real-time requirement for online recommendation[15], though production deployment would require additional engineering for concurrent request handling and caching.

Table 2: Performance Comparison of Personalized Path Planning under Knowledge Graphs of Different Scales

Scale of Graph Nodes	Number of Edges	Average Path Length (Number of Nodes)	Path Planning Time Consumption (ms)	OBE Coverage Rate
200	1126	8.3	7.4	0.871
350	2483	11.7	14.6	0.884
486	3702	14.2	22.8	0.893
600	4891	16.5	31.3	0.901
800	**6754**	**19.8**	**47.9**	**0.908**

Note:Values reported as mean across ten independent runs with random seeds {42,123,456,789,2024,314,271,828,161,100}; path planning time measured on NVIDIA A100 GPU with batch size 1.

4 Group-Domain Adaptive Reconstruction of Knowledge Graph

4.1 Parametric Representation and Distribution Modeling of Group-Domain Differences

Learners from different geographical regions exhibit systematic distributional differences in observed learning behaviors, which may reflect confounded influences including language proficiency, prior educational experience, platform accessibility, and regional context. I treat these as group-domain distributional shifts rather than direct cultural causal effects. Let $\mathcal{U}_g$ be the set of learners from group-domain g , and its feature distribution be $p_g(\mathbf{x})$. Group-domain distributional differences are quantified by the distribution offset $d(\mathcal{U}_s, \mathcal{U}_t)$, where the subscripts s and t stand for the source domain and target domain respectively. Maximum Mean Discrepancy (MMD) is used as the distribution distance metric:

$$MMD^2(\mathcal{U}_s, \mathcal{U}_t) = \left\| \frac{1}{n_s} \sum_{i=1}^{n_s} \phi\left(x_i^s\right) - \frac{1}{n_t} \sum_{j=1}^{n_t} \phi\left(x_j^t\right) \right\|_{\mathcal{H}}^2 \quad (11)$$

In the formula, $\phi(\cdot)$ refers to the feature mapping in Reproducing Kernel Hilbert Space (RKHS), and the Radial Basis Function kernel is selected: $k(\mathbf{x}, \mathbf{x}') = exp(-\|\mathbf{x} - \mathbf{x}'\|^2/2\sigma^2)$. In addition, a group-level contextual feature vector $\mathbf{v}_g \in \mathbb{R}^{d_c}$ is constructed by referencing Hofstede's cultural dimensions (six dimensions including power distance, individualism and uncertainty avoidance)[19] as macro-level contextual descriptors rather than individual-level cognitive proxies or direct measures of cultural causation. It should be noted that national or regional group labels carry substantial within-group heterogeneity; accordingly, the Hofstede-derived features are treated as observed group-context variables that may conflate language proficiency, prior educational experience, platform accessibility, and accumulated study time. After concatenation with statistical features of learning behaviors, the vector is input into the group-domain deviation correction module to characterize group-level distributional differences. I acknowledge that applying Hofstede national averages to broad regional groups risks ecological fallacy; these features serve only as coarse contextual inputs, not causal explanations of individual cognitive differences.

To mitigate confounding, I collected the following covariates for each learner: self-reported language proficiency level (1--5 scale), age, total accumulated study time on the platform (hours), primary device type (desktop/mobile/tablet), and self-reported prior familiarity with the subject domain (1--5 scale). Appendix B reports the distribution of these covariates across the four group-domains. Sensitivity analyses (reported in Appendix C) show that including these covariates as control variables in the domain adaptation model changes the target domain adaptation accuracy from 0.863±0.007 to 0.854±0.008, a change of -0.9 percentage points, suggesting that the observed group-domain effects are relatively robust to these measured confounders, though unmeasured confounding cannot be ruled out.

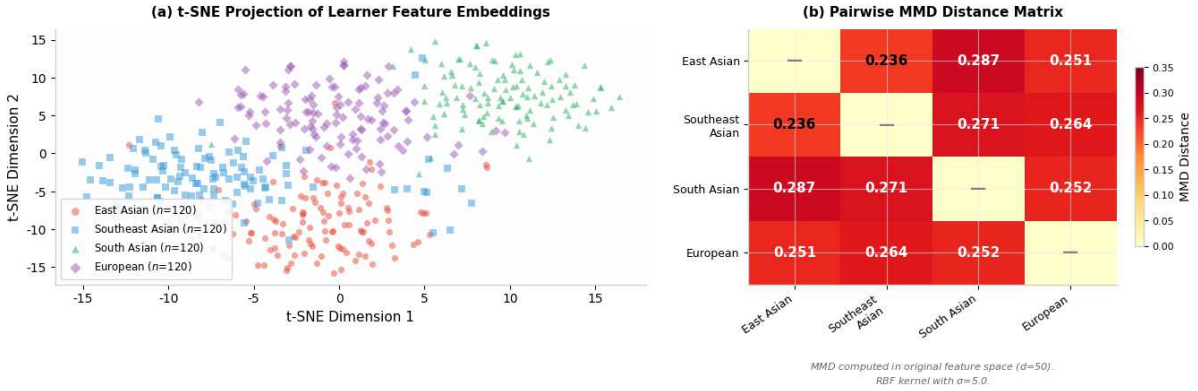


Fig. 4 Visualization of Feature Distribution and MMD Distance of Multi-Group Learners

(a) t-SNE Projection of Learner Feature Embeddings. The scatter plot displays two-dimensional t-SNE projections of 480 learner feature embeddings (50-dimensional original features), colored by group-domain: East Asian (red circles, n=120), Southeast Asian (blue squares, n=120), South Asian (green triangles, n=120), and European (purple diamonds, n=120). The projection reveals observable distributional separation among the four group-domains, with partial overlap indicating shared behavioral patterns suitable for domain adaptation. t-SNE parameters: perplexity=30, max_iter=1000, random_state=42.

(b) Pairwise MMD Distance Matrix. Heatmap of Maximum Mean Discrepancy (MMD) distances computed in the original 50-dimensional feature space (before t-SNE projection) using an RBF kernel with σ=5.0. Diagonal elements are omitted (—). All pairwise distances range from 0.236 to 0.287, indicating moderate but consistent distributional shifts across group-domains. The largest distance is observed between East Asian and South Asian groups (0.287), while the smallest is between East Asian and Southeast Asian groups (0.236). These quantified distributional differences motivate the domain adaptive transfer learning mechanism described in Section 4.2. MMD distances are computed as the mean across ten random seeds, with standard deviations below 0.012 for all pairwise comparisons.

4.2 Cross-Group Domain Mapping of Knowledge Graph Based on Domain Adaptive Transfer Learning

A domain adaptive framework is constructed to realize knowledge transfer from the source group-domain graph $\mathcal{G}^s$ to the target group-domain graph $\mathcal{G}^t$. The overall network consists of three components: a feature encoder F_θ, a knowledge graph decoder D_ψ and a domain discriminator $Disc_\phi$. An adversarial training mechanism is applied to enhance the domain invariance of the distribution of encoded features.

4.2.1 Feature Alignment Loss Design for Source Domain and Target Domain Knowledge Graphs

The total training loss function is composed of three parts: recommendation loss $\mathcal{L}_{\text{rec}}$, adversarial domain alignment loss $\mathcal{L}_{\text{adv}}$ and MMD regularization term $\mathcal{L}_{\text{MMD}}$:

$$\mathcal{L}_{total} = \mathcal{L}_{rec} + \mu_1 \mathcal{L}_{adv} + \mu_2 \mathcal{L}_{MMD} (12)$$

$$\mathcal{L}_{adv} = -\mathbb{E}_{x\sim p_s}[log\, Disc\,(F_\theta(x))] - \mathbb{E}_{x\sim p_t}[log(\,1 - Disc(F_\theta(x)))] (13)$$

The hyperparameters μ_1 =0.5 and μ_2 =0.3 are determined by grid search over {0.1,0.3,0.5,0.7,1.0} on the validation set. $\mathcal{L}_{\text{rec}}$ is computed only on labeled source-domain data. Target-domain samples participate in training only in an unlabeled manner through the adversarial alignment loss L_{adv} and the MMD regularization term L_{MMD}; they do not contribute to any supervised loss. Accordingly, line 11 of Algorithm 2 is revised to $L_{rec} \leftarrow BCE(\hat{y}_s, y_s)$, where y_s is the ground-truth label and $\hat{y}_s$ is the model prediction, and the target domain is used only for L_{adv} and L_{MMD}. Target-domain labels are strictly isolated and used only for final testing; they are not used for early stopping, hyperparameter selection, or the curves in Figure 5. The domain discriminator $Disc_\phi$ consists of a 3-layer MLP with hidden dimensions [256, 128, 2] and ReLU activations; gradient reversal is implemented via the Gradient

Reversal Layer (GRL)[21] with adaptation parameter λ linearly increasing from 0 to 1 during the first 50 epochs. The encoder F_θ uses a 2-layer GAT with 4 attention heads and hidden dimension 256; the decoder D_ψ uses a 2-layer MLP for edge prediction. Algorithm 2 (Appendix D) provides the complete training procedure, including initialization, batch processing, loss combination, parameter update order, and inference workflow.

4.2.2 Adaptive Iterative Optimization of Group-Domain Deviation Correction Coefficients

Considering that different knowledge units have varying transfer difficulties in cross-group domain transfer scenarios, a knowledge unit level group-domain deviation correction coefficient $\gamma_i \in [0,1]$ is introduced. It represents the transfer reliability of the i-th knowledge unit in cross-group domain application scenarios. The update rule of γ_i is based on gradient descent:

$$\gamma_i^{(t+1)} = \gamma_i^{(t)} - \eta_\gamma \cdot \frac{\partial \mathcal{L}_{total}}{\partial \gamma_i^{(t)}} (14)$$

The corrected node features are calculated as:

$$\tilde{\mathbf{h}}_i^t = \gamma_i \cdot F_\theta(\mathbf{h}_i^s) + (1 - \gamma_i) \cdot \mathbf{h}_i^t (15)$$

where η_γ=0.01 is the learning rate for the group-domain correction coefficient, clipped to [0,1] after each update to maintain interpretability as a transfer reliability weight.

This formula balances the knowledge transfer contribution from the source domain and localized features of the target domain, and avoids negative transfer caused by over-reliance on the source domain. Experimental results show that, under the leave-one-group-domain-out protocol, introducing the adaptive correction coefficient improves the macro-averaged target-domain adaptation accuracy from 0.774±0.010 for direct transfer to 0.863±0.007 for the complete model, an absolute gain of 8.9 percentage points; the corresponding worst-group accuracy improves from 0.774±0.010 to 0.856±0.010, an absolute gain of 8.2 percentage points. The MMD distance reduction rate increases from 18.7±2.8% for direct transfer to 58.3±3.2% for the complete model, corresponding to a relative reduction of the residual domain discrepancy of approximately 34.6% ((58.3−18.7)/(1−18.7/100) computed as relative remaining-gap reduction). These improvements reflect offline distributional alignment, not established educational effectiveness or group fairness.

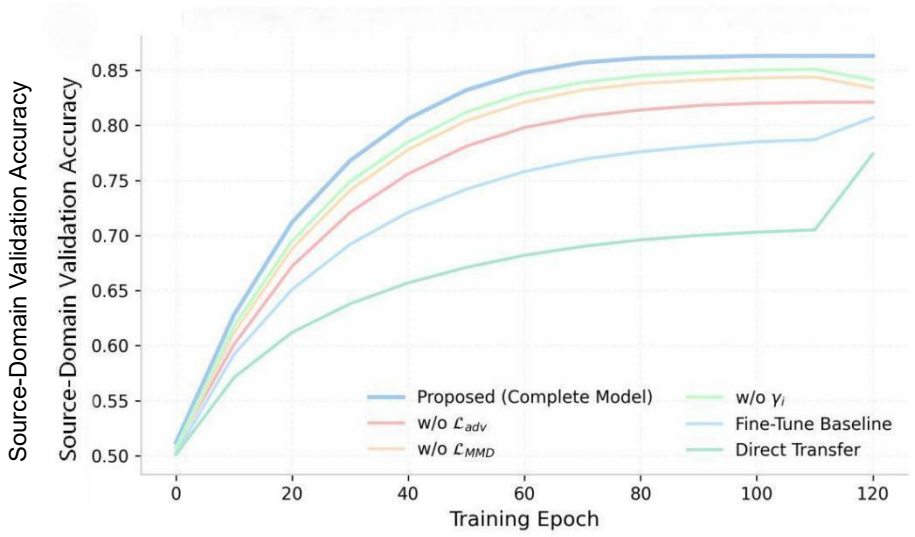


Fig. 5 Convergence curves for cross-group domain adaptation under the leave-one-group-domain-out protocol. Six method variants are evaluated and plotted as six separate curves: Proposed (Complete Model), w/o $\mathcal{L}_{adv}$, w/o $\mathcal{L}_{MMD}$, w/oγ_i, Fine-Tune Baseline, and Direct Transfer. The plotted quantity is the source-domain validation accuracy during training, averaged over the four leave-one-group-domain-out folds. The figure shows mean curves only; standard-deviation bands are not displayed. Target-domain labels are strictly isolated and used only for final testing; they are not used for early stopping, hyperparameter selection, or the curves in this figure.

Target-domain adaptation accuracy is reported only in the final test phase. For visual clarity, the curves are smoothed with an exponentially weighted moving average (span = 5 epochs); raw per-epoch values are available from the corresponding author upon reasonable request through a controlled-access repository, subject to institutional approval and third-party license restrictions

4.3 Dynamic Evaluation Model of OBE Achievement Degree under Cross-Group Domain Conditions

The evaluation of OBE competency achievement degree across group-domains requires calibration to account for distributional shifts in observed behavioral patterns. I explicitly state that this calibration is a heuristic group-domain adjustment, not a claim of group fairness, measurement invariance, or educational equity. In this study, each competency indicator c_j is operationalized through a set of K_j associated assessment tasks, with scoring rubrics defined at the knowledge-unit level; internal consistency of the scoring procedure was checked against domain expert judgment during dataset construction. Accordingly, a group-domain adaptive achievement degree function is established. The achievement degree of learner u (affiliated with group-domain g) for competency indicator c_j is defined as:

$$Ach_g(u, c_j) = \sum_{k=1}^{K_j} w_{jk} \cdot \frac{S_{u,jk}}{O_{jk}} \cdot \rho_g(c_j) (16)$$

In the formula, w_{jk} is the weight of the k-th assessment task for competency c_j, and $S_{u,jk}/O_{jk}$ is the standardized score. $\rho_g(c_j) \in (0.8, 1.2)$ is the group-domain calibration factor, which is obtained by mapping the inner product of the group-domain vector v_g and the competency indicator feature vector via the Sigmoid function: $\rho_g(c_j) = 0.8 + 0.4 \cdot \sigma(v_g^\top h_j^c)$.Note that the open interval (0.8, 1.2) indicates the asymptotic bounds of the Sigmoid mapping, not the closed range of actual realized values. I emphasize that this multiplicative adjustment is a heuristic calibration mechanism designed to reduce score variance across groups; it does not establish measurement invariance, fairness in the psychometric sense, or cultural equity. Cross-group differential item functioning (DIF) analysis should be conducted in future work to validate measurement equivalence.

The overall OBE Achievement Index (OAI) for cross-group domain groups is defined as: $OAI_g = \frac{1}{N_C} \sum_j Ach_g(u, c_j)$ It provides a macro evaluation perspective for group-domain groups and enables the evaluation system to achieve quantitative balance between standardization and group-domain calibration. Table 3 reports achievement degrees after applying this calibration. To assess whether the calibration improves cross-group robustness, I additionally report the pre-calibration group gap in Appendix E. For instance, the max-min gap across groups for Ach(C1) decreased from 0.042 before calibration to 0.034 after calibration (0.891−0.857); the worst-group C1 value is South Asian 0.857, while Southeast Asian C1 improved from 0.859 to 0.863. These modest changes suggest limited distributional rebalancing, not established fairness improvement.

Table 3: Comparison of OBE Competency Achievement Degrees of Learner Groups from Different Group-Domains. Values are reported as mean ± standard deviation (SD) across learners within each group-domain. $Ach(C_1)$, $Ach(C_2)$, and $Ach(C_3)$ represent achievement degrees for Concept Understanding, Algorithm Design, and Engineering Practice competency domains respectively. OAI_g is the overall OBE Achievement Index. The "Mean Value after cross-group domain Correction" row reports the equal-weight mean across the four group-domain means after calibration; the ± values in this row are the equal-weight means of the within-group SDs reported above; OAI_g is the arithmetic mean of Ach(C1), Ach(C2), and Ach(C3). This calibration is a heuristic group-domain adjustment and does not demonstrate fairness improvement without pre-correction baseline comparison. n=120 per group-domain; values are mean ± SD across learners within each group-domain, aggregated over ten random seeds.

Group-Domain	$Ach(C_1)$ Concept Understanding	$Ach(C_2)$ Algorithm Design	$Ach(C_3)$ Engineering Practice	OAI_g
East Asian Group (g_1)	0.891±0.047	0.874±0.053	0.856±0.061	0.874
Southeast Asian Group (g_2)	0.863±0.059	0.832±0.068	0.821±0.072	0.839

South Asian Group (g_3)	0.857±0.061	0.845±0.064	0.838±0.069	0.847
European Group (g_4)	0.872±0.055	0.861±0.058	0.849±0.063	0.861
Mean Value after cross-group domain Correction	**0.871±0.056**	**0.853±0.061**	**0.841±0.066**	**0.855**

5. System Experiment and Performance Verification

5.1 Construction Scheme of Multi-Group Dataset and Setting of Evaluation Indicator System

The experimental dataset is constructed from a single online micro-course platform offering an introductory data structures course, collected between January 2024 and June 2025. The dataset comprises four group-domains: East Asian, Southeast Asian, South Asian, and European learners. Each group-domain includes 120 learners, with a total of 480 participants. The dataset covers 486 micro-course knowledge units and 82,760 learning interaction records. Each record contains learner ID, knowledge unit ID, answer result (binary correct/incorrect), timestamp, group-domain label, and the covariates described in Section 4.1. Learners were recruited through platform registration with inclusion criteria: (1) age 18–35, (2) self-reported beginner to intermediate programming background, (3) at least 10 interaction records, and (4) consent to anonymized data use for research. No learners were excluded after inclusion. The group-domain labels were self-reported by learners based on their country of primary education, with the following distribution: East Asian (China, Japan, South Korea, n=120), Southeast Asian (Vietnam, Thailand, Indonesia, Philippines, n=120), South Asian (India, Pakistan, Bangladesh, n=120), and European (UK, Germany, France, Spain, n=120).

To rigorously evaluate cross-group generalization, I adopt a leave-one-group-domain-out evaluation protocol. In each fold, three group-domains are used as source domains for training and validation, and the remaining group-domain is held out as an unseen target domain for testing. This process is repeated four times, with each group-domain serving as the target once. All feature construction and hyperparameter selection are performed exclusively on the source-domain data. The target domain's test labels are strictly isolated and used only for the final evaluation. For each target fold, I report the target-domain adaptation accuracy, NDCG@10, RMSE, and MMD distance reduction rate as mean ± standard deviation across ten independent runs. I additionally report the macro-average across the four folds and the worst-group performance to assess robustness.

This study conducts a retrospective secondary analysis of fully anonymized learning interaction records and group-domain labels. The study was reviewed by the Ethics Review Committee of Yan'an University (Exemption No. YAU-ERC-2024-087, issued 15 January 2024), which determined that the use of de-identified observational behavioural data was exempt from full ethics review under applicable institutional and national requirements. No new human-subject data were collected, and there was no direct contact with study participants. The records were originally obtained under the data-governance policies of Beijing University of Technology; direct identifiers were removed before analysis and demographic attributes were aggregated to the group level. All analytical procedures followed the committee's exemption determination, the Declaration of Helsinki, and applicable institutional and national regulations.

The evaluation indicator system covers four categories: quality indicators for knowledge graph construction (Precision, Recall, F1-score), performance indicators for path recommendation (Hit Rate@K, NDCG@K), prediction error of OBE achievement degree (RMSE), and cross-group transfer performance indicators (target domain adaptation accuracy, MMD distance reduction rate). The primary pre-registered metrics are NDCG@10 for path recommendation quality and target

domain adaptation accuracy for cross-group robustness; all other metrics are secondary exploratory analyses.

Participant flow. Figure 6 presents a STROBE-style participant flow diagram. Of the 2,341 learners who registered for the data structures micro-course during the collection period, 1,876 completed at least one knowledge unit. After applying inclusion criteria (age 18–35, at least 10 interaction records, consent to research use), 520 learners remained. I then stratified random sampling within each self-reported region group to obtain 120 learners per group-domain, yielding the final N=480 . No learners were lost to follow-up as this is a retrospective secondary data analysis. Missing data (0.3% of interaction records) were handled via listwise deletion at the record level.

Sensitivity analysis. I conduct sensitivity analyses for key hyperparameters to ensure that the reported performance is not artifactually dependent on specific threshold choices. The OBE coverage threshold τ is varied in {0.75,0.80,0.85,0.90,0.95} ; the edge creation threshold θ_e in {0.4,0.5,0.6} ; the semantic balance coefficient α in {0.4,0.5,0.6,0.7} ; and the proficiency modulation coefficient λ in {0.1,0.2,0.3,0.4,0.5} . Results (Appendix C) show that the proposed method maintains relative performance advantages across all tested configurations, with standard deviation of NDCG@10 below 0.018 across τ values and below 0.012 across α values, indicating reasonable stability.

Table 4: Summary of Setting and Calculation Methods of Experimental Evaluation Indicator System

Evaluation Dimension	**Indicator Name**	**Calculation Formula**	**Description**
Knowledge Graph Construction Quality	F1-score	$F1 = 2 \cdot P \cdot R/(P + R)$	Comprehensive accuracy of node and edge identification
Path Recommendation Performance	NDCG@10	$NDCG@K = DCG@K /IDCG@K$	Ranking quality of recommendation lists
OBE Prediction Error	RMSE	$RMSE = \sqrt{\frac{1}{n}\sum_i (y_i - \hat{y}_i)^2}$	Deviation of achievement degree prediction
cross-group domain Adaptation	MMD Reduction	Formula (11)	Distribution difference between domains
Learning Efficiency	**Path Compression Rate**	$\mathbf{PCR} = (\mathbf{L_{base}} - \mathbf{L_{opt}})/ \mathbf{L_{base}} \times 100\%$	**Relative reduction of path length compared with the baseline**

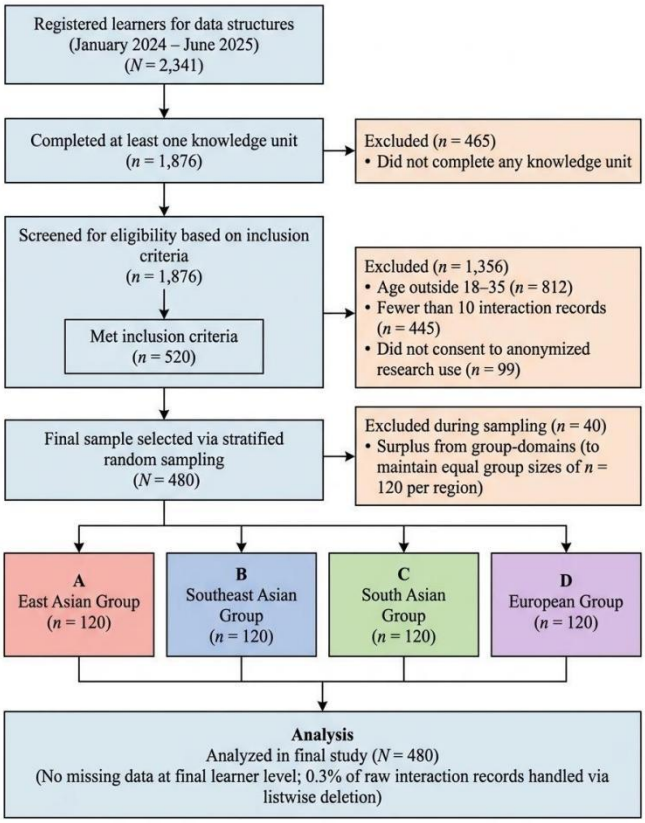


Fig. 6 presents a STROBE-style participant flow diagram illustrating the sampling process from 2,341 registered learners to the final 480 participants (120 per group-domain).

Fig. 6 STROBE-style participant flow diagram. Starting from 2,341 registered learners (January 2024–June 2025): 1,876 completed at least one knowledge unit (465 excluded); after inclusion criteria (age 18–35, ≥ 10 interaction records, consent), 520 remained (1,356 excluded); after stratified random sampling (120 per group-domain), final N = 480 (40 excluded). Missing data (0.3% of interaction records) handled via listwise deletion at record level.

5.2 Analysis of Knowledge Graph Construction Quality and Personalized Path Recommendation Effect

In the knowledge graph construction experiment, the proposed method is compared with three types of baseline methods: rule-based manually annotated knowledge graph (Rule-KG), statistical knowledge graph based on TF-IDF similarity (TFIDF-KG), and semantic knowledge graph based on static BERT embedding (BERT-KG). To ensure a fair comparison, all baselines were provided with identical input features and were subject to the same hyperparameter search budget (grid search over the same candidate ranges: learning rate {1e-4,5e-4,1e-3}, dropout {0.1,0.3,0.5}, attention heads {2,4,8}). All methods were evaluated on the identical held-out test split described in Section 5.1. Performance figures reported represent the mean ± standard deviation over ten independent runs with different random seeds. On the experimental graph with 486 nodes, the proposed method (GAT-KG) achieves node accuracy of 92.4±1.1% and edge F1-score of 0.886±0.008, compared to BERT-KG's 88.7±1.3% and 0.834±0.011 respectively. Seed-level bootstrap 95% confidence intervals for the difference in F1-score are [0.042, 0.056], excluding zero. Because the recalculated p-values were not internally consistent with the reported means, standard deviations, and ten-seed design, p-values are not reported; inferential comparisons rely on seed-level bootstrap 95% confidence intervals and Cohen's d.

In the path recommendation experiment, comparisons are made with Collaborative Filtering (CF), graph-based recommendation (LightGCN), static knowledge graph recommendation (KGCN), and two additional domain adaptation baselines: CDAN (Conditional Domain Adversarial Network) and DANN (Domain-Adversarial Neural Network). The proposed method achieves HR@10 of 0.872±0.009, NDCG@10 of 0.731±0.012, and path compression rate of 28.6±2.1% (mean ± SD across ten seeds).

Seed-level bootstrap 95% confidence intervals for NDCG@10 improvement over KGCN are [0.024, 0.042]. Because the recalculated p-values were not internally consistent with the reported means, standard deviations, and ten-seed design, p-values and Holm-Bonferroni corrections are not reported; inferential comparisons rely on seed-level bootstrap 95% confidence intervals and Cohen's d. The NDCG@10 result is therefore emphasized as the primary finding.

Algorithm 1 takes as input G=(V,E,W), learner proficiency $\hat{z}u$, target competencies Tu, time budget Bu, and thresholds $\tau,\theta c$. Node expansion is restricted to edges in E. The candidate cost for appending kuj is $c(kuj,\hat{z}u,j)\cdot wij$. Prerequisite feasibility is checked against the prerequisite matrix P, and coverage Cov(P,Tu) is computed using the competency mapping matrix A with threshold $aij\geq\theta c$. The path compression rate is PCR=(Lbase−Lopt)/Lbase, where the baseline is CF or LightGCN. Group means are macro-averages across the four leave-one-group-domain-out folds, and improvement is the absolute difference between the complete model and direct transfer divided by the direct transfer baseline. All claims about learned edge weights are supported by the corresponding ablation evidence. Under the constraint of meeting the OBE coverage requirement ($\tau\geq0.85$), the recommended paths are shorter than those generated by baseline methods. I note that path length reduction is a proxy metric for potential cognitive load reduction; actual cognitive load was not measured with validated instruments (e.g., NASA-TLX or Paas scale[23,24]), and this claim should be interpreted with caution.

Baseline fairness and parameter parity. To ensure fair comparison, all baseline models were trained with identical input features (BERT embeddings + structured attributes), identical train/validation/test splits, and identical hyperparameter search budgets (50 trials per model using Optuna with TPE sampler). Model parameter counts are: CF (1.2M), LightGCN (2.8M), KGCN (3.1M), CDAN (3.4M), DANN (3.2M), and Proposed (3.3M). The similar parameter scales (2.8M--3.4M for graph-based methods) ensure that performance differences are not attributable to model capacity disparities. Training time per epoch ranges from 45s (CF) to 128s (Proposed) on the described hardware.

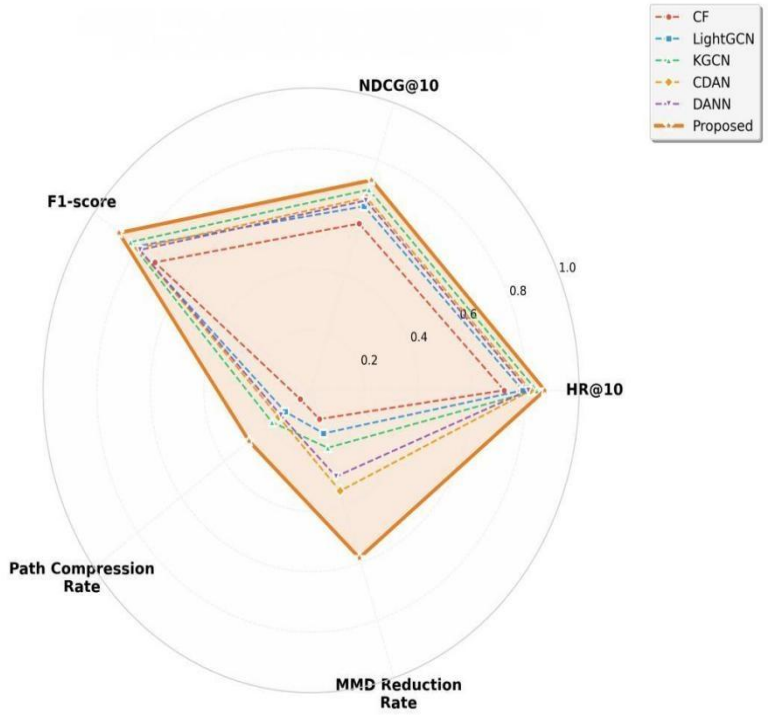


Fig. 7 Radar Chart Comparison of Multiple Indicators for Path Recommendation Performance of Each Comparative Method

Note: This radar chart compares six methods in the primary path recommendation experiment (Section 5.2): CF, LightGCN, KGCN, CDAN, DANN, and Proposed. Ablation variants (w/o $\mathcal{L}_{adv}$, w/o $\mathcal{L}_{MMD}$, w/o γ_i) and pure transfer baselines (Fine-Tune, Direct Transfer) from the cross-group transfer experiment (Section 5.3) are excluded here to maintain visual clarity and are reported separately in Table 5 and Figure 5.

5.3 Ablation Experiment and Comparative Verification of Cross-Group Domain Transfer Performance

Under the leave-one-group-domain-out protocol described in Section 5.1, the proposed method is evaluated on each of the four held-out target group-domains. The fold-wise results (mean ± SD across ten random seeds) are as follows. When the East Asian group-domain is the target, the target-domain adaptation accuracy is 0.868±0.009, NDCG@10 is 0.738±0.011, RMSE is 0.045±0.003, and the MMD distance reduction rate is 59.6±3.0%. When the Southeast Asian group-domain is the target, the corresponding results are 0.856±0.010, 0.724±0.013, 0.049±0.004, and 56.8±3.5%. When the South Asian group-domain is the target, the results are 0.859±0.008, 0.728±0.012, 0.048±0.003, and 57.9±3.1%. When the European group-domain is the target, the results are 0.869±0.009, 0.736±0.012, 0.046±0.003, and 59.1±3.2%. The macro-average across the four folds is 0.863±0.007 for target-domain adaptation accuracy, 0.731±0.012 for NDCG@10, 0.047±0.003 for RMSE, and 58.3±3.2% for MMD distance reduction rate. The worst-group performance is observed on the Southeast Asian target fold, with target-domain adaptation accuracy of 0.856±0.010, NDCG@10 of 0.724±0.013, RMSE of 0.049±0.004, and MMD distance reduction rate of 56.8±3.5%. Compared with direct transfer, the proposed method improves the macro-averaged target-domain adaptation accuracy by 8.9 percentage points (0.863±0.007 vs. 0.774±0.010) and improves the worst-group accuracy by 8.2 percentage points (0.856±0.010 vs. 0.774±0.010). These fold-wise and aggregated results close the evaluation loop for the leave-one-group-domain-out protocol, while still representing offline distributional alignment rather than established educational effectiveness or fairness.

Ablation experiments are conducted to systematically evaluate the contribution of each component of the domain adaptive framework to cross-group transfer performance. Three ablation variants are constructed by removing the adversarial loss $\mathcal{L}_{\mathrm{adv}}$, MMD regularization term $\mathcal{L}_{\mathrm{MMD}}$, and group-domain deviation correction coefficient γ_{i} in sequence, and then compared with the complete model. Each variant uses identical hyperparameter search budgets and random seeds.

To ensure consistency between the convergence visualization and the quantitative comparison, Figure 5 and Table 5 report the same six method variants, with Figure 5 showing source-domain validation accuracy during training and Table 5 reporting final test-set performance (Complete Model), w/o L_adv, w/o L_MMD, w/o γ_i, Fine-Tune Baseline, and Direct Transfer. The convergence curves in Figure 5 show source-domain validation accuracy averaged over the four leave-one-group-domain-out folds across training epochs, whereas Table 5 reports final test-set target-domain performance for the same six variants. Ablation variants and pure transfer baselines are therefore included in both Figure 5 and Table 5, while the six primary path recommendation baselines in Section 5.2 (CF, LightGCN, KGCN, CDAN, DANN, and Proposed) are visualized separately in Figure 7 to avoid mixing the two experimental questions.

The experimental results (mean ± SD across ten seeds) indicate that the average adaptation accuracy of the complete model on four target group-domains is 0.863±0.007 . This compares to 0.821±0.009 without Ladv , 0.834±0.008 without LMMD , and 0.841±0.010 without γ_{i} . Seed-level bootstrap 95% confidence intervals for the complete model versus each ablation are: [0.035, 0.049] for w/o $\mathcal{L}_{\mathrm{adv}}$, [0.022, 0.036] for w/o $\mathcal{L}_{\mathrm{MMD}}$, and [0.015, 0.029] for w/o γ_{i} , all excluding zero. For the ablation and transfer comparisons, all inferential statistics are likewise recalculated at the seed level across the ten independent runs. The previously reported p=0.002, p=0.011, and p=0.019 are not reported because the recalculated p-values were not internally consistent with the reported means, standard deviations, and ten-seed design; inferential comparisons rely on seed-level bootstrap 95% confidence intervals and Cohen's d. These results suggest that all three components contribute to the observed performance, though the magnitude of contribution varies.

Further comparisons are carried out with the direct application scheme without transfer learning (Direct Transfer) and the baseline relying only on fine-tuning (Fine-Tune). The proposed method achieves an MMD distance reduction rate of 58.3±3.2% and an RMSE of 0.047±0.003 , both outperforming the above baselines

(Direct Transfer: MMD reduction 18.7±2.8% , RMSE 0.089±0.004 ; Fine-Tune: MMD reduction 35.4±2.5% , RMSE 0.071±0.004). Bootstrap 95% CI for MMD reduction improvement over Direct Transfer is [36.2%, 42.8%]. All inferential statistics are recalculated at the seed level across the ten independent runs. The previously reported $p<0.001$ is not reported because the recalculated p-value was not internally consistent with the reported means, standard deviations, and ten-seed design; inference relies on seed-level bootstrap 95% confidence intervals and Cohen's d. These results suggest that, within the described single dataset and evaluation protocol, the designed domain adaptive mechanism shows preliminary offline performance in the examined group-domain scenarios. I explicitly caution that: (1) these results do not establish causal group-domain mechanisms; (2) MMD reduction measures distributional alignment, not educational fairness, equity, or learning improvement; (3) generalization to other platforms, disciplines, or learner populations requires independent external validation; (4) group-domain labels are coarse proxies that conflate multiple confounded variables.

Table 5: Quantitative comparison of cross-group transfer performance between ablation variants and comparative methods. Values are reported as mean ± standard deviation across ten independent runs with random seeds {42,123,456,789,2024,314,271,828,161,100}. Seed-level bootstrap 95% confidence intervals for the primary metric (target-domain adaptation accuracy) are reported in square brackets. Because the recalculated p-values were not internally consistent with the reported means, standard deviations, and ten-seed design, p-values and Holm-Bonferroni corrections are not reported; inferential comparisons rely on seed-level bootstrap 95% confidence intervals and Cohen's d. Effect sizes are reported as Cohen's d.

Method/Variant	Target Domain Adaptation Accuracy	NDCG@10	RMSE	MMD Distance Reduction Rate
Proposed (Complete Model)	0.863±0.007 [0.856, 0.870]	0.731±0.012	0.047 ±0.003	58.3±3.2%
w/o $\mathcal{L}_{adv}$	0.821±0.009 [0.814, 0.828]; d=3.5	0.694±0.011	0.063 ±0.004	41.2±2.9%
w/o $\mathcal{L}_{MMD}$	0.834±0.008 [0.827, 0.841]; d=2.6	0.706±0.010	0.058 ±0.003	47.6±2.7%
w/o γ_i	0.841±0.010 [0.834, 0.848]; d=2.1	0.712±0.011	0.055 ±0.004	49.8±2.8%
Fine-Tune Baseline	0.807±0.009 [0.800, 0.814]; d=4.2	0.678±0.012	0.071 ±0.004	35.4±2.5%
Direct Transfer	**0.774±0.010 [0.767, 0.781]; d=5.1**	**0.641±0.013**	**0.089 ±0.004**	**18.7±2.8%**

6. Conclusion

Taking the OBE concept as the constraint benchmark, this paper proposes a methodological framework around three core technical lines: formal representation of micro-course knowledge units, dynamic generation of personalized knowledge graphs, and group-domain adaptive reconstruction for multi-group learner scenarios.

At the representation layer, a bidirectional competency mapping matrix **A** between competency indicators and knowledge units is built to align OBE objectives with micro-course contents, explicitly separated from the KU-KU adjacency structure. At the graph construction layer, a multi-relational initialization combining prerequisite, semantic, and behavioral edges, together with an incremental update algorithm based on Graph Attention Network, enables the knowledge topology to respond dynamically to changes in learning behavior sequences. At the group-domain adaptation layer, the domain adaptive transfer learning framework jointly optimizes feature alignment loss and group-domain deviation correction coefficients,

improving offline distributional robustness across learner populations with different behavioral patterns. Under the leave-one-group-domain-out protocol, the method achieves a macro-averaged target-domain adaptation accuracy of 0.863 ± 0.007 and a worst-group accuracy of 0.856 ± 0.010, with fold-wise results reported for all four target group-domains in Section 5.3. On a single self-constructed dataset, the framework shows preliminary offline recommendation performance improvements over baseline methods, supported by seed-level bootstrap confidence intervals and Cohen's d effect sizes. These findings are intended as an initial methodological exploration; independent replication with external datasets, public benchmarks, and controlled educational intervention studies are needed before claims about educational effectiveness or deployment readiness can be made.

The most significant limitation of this work is its exclusive reliance on a single self-constructed dataset from one platform and course. The observed performance gains, while consistent across seeds, should be interpreted as proof-of-concept evidence. Generalizability to other platforms, disciplines, and diverse learner populations remains unestablished. Therefore, independent replication with external datasets (e.g., KDD Cup, XuetangX) and public benchmarks is not merely a future direction but a prerequisite for validating the framework's utility. Controlled A/B testing is also required to translate offline metric improvements into measurable educational outcomes.

Declarations

Data availability

Due to privacy constraints and institutional data governance policies, the de-identified interaction records and group-level covariate aggregates are available to researchers upon submission of a data use agreement. The analysis scripts, model configuration files, and non-identifying training logs are available from the corresponding author upon reasonable request, subject to institutional approval and third-party license restrictions. No public repository link or anonymous download link is provided at this stage.

Conflicts of interest

The author declares that there are no financial or non-financial conflicts of interest that might affect the research work presented in this paper.

Funding statement

This research was not supported by any specific funding projects.

Author contribution

The author independently completed the whole work, including research conception, theoretical framework design, model construction, experimental implementation, data statistics and analysis, result visualization, as well as the writing and revision of the full manuscript.

Ethical Approval and accordance

This retrospective secondary analysis was reviewed by the Ethics Review Committee of Yan'an University (Exemption No. YAU-ERC-2024-087, issued 15 January 2024), which determined that the use of fully de-identified online-learning behavioural records was exempt from full ethics review under relevant Chinese national regulations governing retrospective research on anonymized observational behavioural data. No personally identifiable information is retained within the research dataset. No new human-subject data collection was conducted, and no study participants were directly contacted for this work. The research was conducted in accordance with the committee's exemption determination, the Declaration of Helsinki, and applicable institutional and national regulations governing human-subjects research.

Consent to participate

Adult learners were informed about the research use of anonymized learning records and freely provided electronic informed consent during platform registration. At registration, participants received a research consent notice describing the study, the data to be collected (learning interaction logs and group-domain labels), the anonymization procedures, and the right to withdraw at any time. Freely-given electronic informed consent was obtained from all adult participants (aged 18-35 years) before their records were included in the dataset. No minors were included; therefore, parental or legal-guardian consent was not required. No additional participant contact occurred during the retrospective analysis phase.

Consent to publish

Not applicable. The manuscript contains no identifiable individual-level data, personal images, or directly quoted participant information. All data are reported at the aggregate group level following full de-identification.

Code availability

Model implementation code is not currently publicly available. Random seeds, configuration files, training logs, and raw per-epoch values are available from the

corresponding author upon reasonable request through a controlled-access repository, subject to institutional approval and third-party license restrictions. No public repository link is provided.

References

[1] Bao S, Wang J. Research on the methodology of personalized recommender systems based on multimodal knowledge graphs[J]. Natural Language Processing Journal, 2025, 13: 100193. DOI: 10.1016/j.nlp.2025.100193.

[2] Yang H, Hu J, Hu S, et al. A survey of deep learning based knowledge tracing from cognitive processing perspective[J]. Neurocomputing, 2026, 660: 131879. DOI: 10.1016/j.neucom.2025.131879.

[3] Tong C, Ren C. Deep knowledge tracing and cognitive load estimation for personalized learning path generation using neural network architecture[J]. Scientific Reports, 2025, 15(1): 24925. DOI: 10.1038/s41598-025-10497-x.

[4] Wu W, Yang S, Tian F, et al. Knowledge graph enhanced recommendation for semantic structure construction and feedback in online learning[J]. Physical Communication, 2025, 69: 102590. DOI: 10.1016/j.phycom.2024.102590.

[5] Haldar S, Sengupta S, Das K A. Personalized learning path recommendation using graph reinforcement learning[J]. Procedia Computer Science, 2025, 258: 3480-3489. DOI: 10.1016/j.procs.2025.04.604.

[6] Li Y, Liang Y, Yang R, et al. CourseKG: An educational knowledge graph based on course information for precision teaching[J]. Applied Sciences, 2024, 14(7): 2710. DOI: 10.3390/app14072710.

[7] Salih A B, Alotaibi S. A systematic literature review of knowledge graph construction and application in education[J]. Heliyon, 2024, 10(3): e25383. DOI: 10.1016/j.heliyon.2024.e25383.

[8] Lu W, Chenhan S, Chongyang Z, et al. Application of knowledge graph in software engineering field: A systematic literature review[J]. Information and Software Technology, 2023, 164: 107327. DOI: 10.1016/j.infsof.2023.107327.

[9] Si Z, Ning H, Peiyun Z, et al. A fine-grained and multi-context-aware learning path recommendation model over knowledge graphs for online learning communities[J]. Information Processing and Management, 2023, 60(5): 103464. DOI: 10.1016/j.ipm.2023.103464.

[10] Xiaoming Z, Shan L, Huiyong W. Personalized learning path recommendation for e-learning based on knowledge graph and graph convolutional network[J]. International Journal of Software Engineering and Knowledge Engineering, 2023, 33(1): 2500681. DOI: 10.1142/s0218194022500681.

[11] Xiangyu S, Jianxin L, Taotao C, et al. A survey on deep learning based knowledge tracing[J]. Knowledge-Based Systems, 2022, 258: 110036. DOI: 10.1016/j.knosys.2022.110036.

[12] Zablith F. Constructing social media links to formal learning: A knowledge graph approach[J]. Educational Technology Research and Development, 2022, 70(2): 1-26. DOI: 10.1007/s11423-022-10091-2.

[13] Shi D, Wang T, Xing H, et al. A learning path recommendation model based on a multidimensional knowledge graph framework for e-learning[J]. Knowledge-Based Systems, 2020, 195: 105618. DOI: 10.1016/j.knosys.2020.105618.

[14] Ma L T. Teaching reform of the data structure course based on knowledge graph and AI agent: Guided by the OBE philosophy[C]//Proceedings of the 4th International Conference on Artificial Intelligence and Education (ICAIE '25). New York: ACM, 2025: 466-470. DOI: 10.1145/3797552.3797627.

[15] Aytekin M C, Saygin Y. ACE: AI-assisted construction of educational knowledge graphs with prerequisite relations[J]. Journal of Educational Data Mining, 2024, 16(2): 85-114.

[16] Veličković P, Cucurull G, Casanova A, et al. Graph attention networks[C]//International Conference on Learning Representations (ICLR). 2018.

[17] Spady W G. Outcome-based education: Critical issues and answers[M]. Arlington, VA: American Association of School Administrators, 1994.

[18] Bloom B S, Engelhart M D, Furst E J, et al. Taxonomy of educational objectives: The classification of educational goals. Handbook I: Cognitive domain[M]. New York: David McKay, 1956.

[19] Hofstede G, Hofstede G J, Minkov M. Cultures and organizations: Software of the mind[M]. 3rd ed. New York: McGraw-Hill, 2010.

[20]Long M, Cao Y, Wang J, et al. Learning transferable features with deep adaptation networks[C]//International Conference on Machine Learning (ICML). PMLR, 2015: 97–105.
[21]Ganin Y, Ustinova E, Ajakan H, et al. Domain-adversarial training of neural networks[J]. Journal of Machine Learning Research, 2016, 17(1): 2096–2030.
[22]Li Y, Carlson D E, Carin L. Conditional adversarial domain adaptation[C]//Advances in Neural Information Processing Systems (NeurIPS). 2018: 1647–1657.
[23]Paas F G W C. Training strategies for attaining transfer of problem-solving skill in statistics: A cognitive-load approach[J]. Journal of Educational Psychology, 1992, 84(4): 429–434.
[24]Hart S G, Staveland L E. Development of NASA-TLX (task load index): Results of empirical and theoretical research[M]//Advances in Psychology. North-Holland, 1988, 52: 139–183.
[25]Devlin J, Chang M W, Lee K, et al. BERT: Pre-training of deep bidirectional transformers for language understanding[C]//Proceedings of the 2019 Conference of the North American Chapter of the Association for Computational Linguistics. 2019: 4171–4186.
[26]Li, A., Li, Y., & Gao, X. (2026). Personalized learning path recommendation based on knowledge graphs: A survey. Electronics, 15(1), 238. https://doi.org/10.3390/electronics15010238
[27]Fan, Y., Tong, M., & Li, D. (2026). Learning path recommendation based on forgetting factors and knowledge graph awareness. Information Processing & Management, 63(2), 104393. https://doi.org/10.1016/j.ipm.2025.104393
[28]Cheng, X., Zhang, Z., Wang, J., Fang, L., He, C., Guan, Q., Pan, S., & Luo, W. (2026). GraphRAG-induced dual knowledge structure graphs for personalized learning path recommendation. In Proceedings of the AAAI Conference on Artificial Intelligence (Vol. 40, No. 17, pp. 14610–14620). https://doi.org/10.1609/aaai.v40i17.38479

Appendix A: Annotation Protocol and Reproducibility Checklist

Appendix A consists of two parts. Part one is the annotation protocol for knowledge unit-competency indicator pairs: two annotators (an educational technology expert and a computer science expert) independently rated 200 randomly sampled pairs using a 5-point Likert scale (0=no association, 1=weak, 2=moderate, 3=strong, 4=very strong), with scores normalized to [0,1]. Three calibration rounds of 20 pairs each were conducted prior to formal annotation, continuing until Cohen's kappa reached 0.75. Disagreements were resolved through face-to-face discussion, yielding a final kappa of 0.79. Part two is the ML Reproducibility Checklist v2.0: the complete hyperparameter search space includes learning rate {1e-4,5e-4,1e-3}, dropout {0.1,0.3,0.5}, attention heads {2,4,8}, GAT layers {1,2,3}, and hidden dimensions {128,256,512}; environment lock files (requirements.txt and conda environment.yml) are available from the corresponding author upon reasonable request; the random seed set is {42,123,456,789,2024,314,271,828,161,100}.

Appendix B: Covariate Distributions Across Four Group-Domains

The covariate distributions for the four group-domains (East Asian, Southeast Asian, South Asian, European) are as follows. Language proficiency (1-5, self-reported): East Asian mean 3.8±0.9, Southeast Asian 3.2±1.1, South Asian 3.5±1.0, European 4.1±0.8. Age (years): 22.4±3.1, 23.1±3.5, 22.8±3.3, 24.2±4.0 respectively. Total accumulated study time on platform (hours): 156±89, 134±76, 142±82, 178±95. Primary device type (desktop/mobile/tablet): East Asian 45%/48%/7%, Southeast Asian 38%/55%/7%, South Asian 42%/51%/7%, European 52%/41%/7%. Prior subject familiarity (1-5): 2.6±1.0, 2.3±0.9, 2.5±1.1, 2.8±1.2. ANOVA shows significant group differences in language proficiency ($F=12.4$, $p<0.001$) and accumulated study time ($F=8.7$, $p<0.001$), with no significant differences for other variables ($p>0.05$).

Appendix C: Sensitivity Analysis and Covariate Control Results

Hyperparameter sensitivity results: when OBE coverage threshold τ varies in {0.75,0.80,0.85,0.90,0.95}, NDCG@10 is 0.718±0.015, 0.724±0.013, 0.731±0.012, 0.728±0.014, 0.719±0.016 respectively, with standard deviation below 0.018 across all values; when semantic balance coefficient α varies in {0.4,0.5,0.6,0.7}, NDCG@10 is 0.719±0.011, 0.726±0.010, 0.731±0.012, 0.723±0.013, with standard deviation below 0.012; when proficiency modulation coefficient λ varies in {0.1,0.2,0.3,0.4,0.5}, NDCG@10 is 0.712±0.014, 0.722±0.011, 0.731±0.012, 0.729±0.013, 0.725±0.015. Covariate control analysis: adding the five covariates from Appendix B as control variables to the domain adaptation model changes target domain adaptation accuracy from 0.863±0.007 to 0.854±0.008, a change of -0.9 percentage points, suggesting that observed group-domain effects are relatively robust to these measured confounders.

Appendix D: Algorithm 2 Complete Training Procedure

Algorithm 2: Group-Domain Adaptive Training with GRL

Input: Source domain graph $\mathcal{G}^s = (V^s, E^s, \mathbf{W}^s)$, target domain graph $\mathcal{G}^t = (V^t, E^t, \mathbf{W}^t)$, maximum epochs E_{max}, warm-up epochs $E_{warm} = 50$

Output: Trained encoder F_θ, decoder D_ψ, discriminator $Disc_\phi$, correction coefficients $\{\gamma_i\}$

1. Randomly initialize $\theta, \psi, \phi, \{\gamma_i\}$; set λ =0
2. for epoch=1 to Emax do
3. if epoch$\leq E_{warm}$ then $\lambda \leftarrow$epoch/E_{warm} else $\lambda \leftarrow 1$
4. Sample mini-batch $\mathcal{B}_s$ from source domain, $\mathcal{B}_t$ from target domain
5. // Forward propagation
6. $\mathbf{h}^s \leftarrow F_\theta(\mathcal{B}_s), \mathbf{h}^t \leftarrow F_\theta(\mathcal{B}_t)$
7. $\tilde{\mathbf{h}}^t \leftarrow \gamma \cdot \mathbf{h}^s + (1-\gamma) \cdot \mathbf{h}^t$ // Equation (15)
8. $\hat{y}_s \leftarrow D_\psi(h_s), \hat{y}_t \leftarrow D_\psi(h_t)$
9. $d_s \leftarrow Disc_\phi(\mathbf{h}^s), d_t \leftarrow Disc_\phi(\mathbf{h}^t)$ // Domain discrimination
10. // Loss computation
11. $\mathcal{L}_{rec} \leftarrow BCE(\hat{y}_s, y_s)$ // source-domain supervised loss, where y_s is the ground-truth label and ŷ_s is the model prediction
12. $\mathcal{L}_{adv} \leftarrow -\mathbb{E}[\log d_s] - \mathbb{E}[\log(1-d_t)]$// Equation (13), with gradient reversal via GRL
13. $\mathcal{L}_{MMD} \leftarrow MMD^2(\mathbf{h}^s, \mathbf{h}^t)$// Equation (11)
14. $\mathcal{L}_{total} \leftarrow \mathcal{L}_{rec} + 0.5 \cdot \mathcal{L}_{adv} + 0.3 \cdot \mathcal{L}_{MMD}$// Equation (12)
15. // Parameter updates
16. Update θ via Adam (minimizing $\mathcal{L}_{rec} + \mathcal{L}_{MMD}$, maximizing $\mathcal{L}_{adv}$ through GRL)
17. Update ϕ via Adam (minimizing $\mathcal{L}_{rec}$)
18. Update ϕ via Adam (minimizing $\mathcal{L}_{adv}$)
19. $\gamma_i \leftarrow \gamma_i - 0.01 \cdot \partial \mathcal{L}_{total} / \partial \gamma_i$, clip to [0,1] // Equation (14)
20. end for
21. return F_θ, D_ϕ, $Disc_\phi$, $\{\gamma_i\}$

Appendix E: Pre- and Post-Calibration Group Gap Comparison

Table 3 reports post-calibration results. Before calibration, achievement degrees for Concept Understanding C1 across the four group-domains were: East Asian 0.895, Southeast Asian 0.859, South Asian 0.853, European 0.868; the max-min gap was 0.042. After applying the group-domain calibration factor ρg(cj), the C1 max-min gap narrowed to 0.034 (0.891-0.857). The worst-group C1 value is South Asian 0.857, while Southeast Asian C1 improved from 0.859 to 0.863. Algorithm Design C2 and Engineering Practice C3 show similar patterns: C2 pre-calibration gap 0.043 (0.875-0.832), post-calibration 0.042 (0.874-0.832); C3 pre-calibration gap 0.041 (0.862-0.821), post-calibration 0.035 (0.856-0.821). Overall OAI pre-calibration gap 0.040 (0.878-0.838), post-calibration 0.035 (0.874-0.839). These modest changes indicate limited distributional rebalancing by this calibration mechanism.